Sigma Journal of Engineering and Natural Sciences
Web page info: https://sigma.yildiz.edu.tr
DOI: 10.14744/sigma.2022.00004

Research Article

Comparison of post and iris substrate integrated waveguide band-pass filters for X-Band applications

Hammam BANDAR[1], Nurhan TÜRKER TOKAN[1]*

[1]*Department of Electronics and Communications Engineering, Yildiz Technical University, Istanbul, Turkey*

ARTICLE INFO

Article history
Received: 10 November 2020
Accepted: 25 January 2021

Key words:
Band-pass filter; Centered post filter; Iris filter; SIW

ABSTRACT

The substrate integrated waveguide (SIW) has been proposed as a reliable alternative to the rectangular waveguide due to its small size, low cost, high performance, ease of manufacturing and simplicity of integration with other microwave components. This paper focuses on SIW band-pass filters and presents their design procedure in details. The methodology is applied to post and iris SIW filters working at X-band with different orders, responses and bandwidths. Two prototypes of third-order post and iris SIW filters are fabricated and measured with a vector network analyzer. The filters are designed to work at 10 GHz center frequency and 500 MHz bandwidth. The simulation results and measurement results of the post and iris SIW filters are compared. In the simulations lower than 0.9 dB insertion loss and better than 20 dB return loss is observed in the pass-band of the filters. The post filter exhibits lower insertion loss and higher reflection loss at the stop-band of the filter. With their low cost, small size, ease of manufacturing, high performance and integrability with other components, both of the demonstrated X-band SIW filters are very versatile and well suited for a variety of market applications, including radars and satellite communications.

Cite this article as: Bandar H, Türker Tokan N. Comparison of post and iris substrate integrated waveguide band-pass filters for X-Band applications. Sigma J Eng Nat Sci 2022;40(1):45–56

INTRODUCTION

Microwave filters have been in the picture for a long time and have been playing an important role in civilian applications and military systems such as wireless computer networks, military and government radar applications, including weather monitoring, air traffic control, maritime vessel traffic control, defense tracking and vehicle speed detection [1-2]. Since the electromagnetic spectrum is limited, the channel bandwidth became a scarce resource [3]. Therefore, the role of microwave filters became very important in the mentioned applications. In these applications, tighter specifications for microwave filters are required. To that end, the most commonly used filters are band-pass

***Corresponding author.**
*E-mail address: nturker@yildiz.edu.tr

This paper was recommended for publication in revised form by Regional Editor N. Özlem Ünverdi

Published by Yıldız Technical University Press, İstanbul, Turkey

filters (BPFs). Depending on BPF application, parameters like insertion loss, return loss, bandwidth and attenuation require careful optimization steps.

As frequency increases, transmission loss increases, and the amount of energy emergence decreases [1]. As a result, hollow-pipe waveguides such as rectangular waveguides (RWs) are preferred. RWs and RW filters are necessary and fundamental components in various practical microwave and millimeter-wave applications, especially for communication systems that require low loss and high power handling capability at higher frequencies like radar communications, satellite communications and mobile radio communications [4-6]. However, RW filters have the disadvantages such as bulky size, difficulty of manufacturing, high cost and difficulty of integration with printed structures due to the need of complex transitions [7-8].

Due to the necessity for miniaturization and integration, planar transmission lines like the microstrip line and stripline are used instead of RWs for many applications. However, these structures have high loss and low power handling capability. As a result, to overcome these difficulties, substrate integrated waveguide (SIW), which combines the advantages of waveguides with the advantages of planar transmission lines, has been proposed [8-9]. SIW has crucial properties such as small size, ease of manufacturing, low cost, high performance, high power handling capacity, low interference and simplicity of integration with other microwave components [10].

SIW belongs to the family of substrate integrated circuits (SICs) [11-12]. Its structure consists of two arrays of metallic via-holes parallel to each other embedded in a dielectric substrate that electrically connect two parallel metal plates (upper and lower) [13-14]. These via-holes are equivalent to the two metal sidewalls of the RW, while the top and bottom layers of SIW are equivalent to the upper and lower RW walls [15]. When compared to microstrip and waveguide structures, a SIW has the characteristic of having no additional components and can be easily realized with a conventional standard printed circuit board (PCB) process, thick film process or low-temperature co-firing ceramic (LTCC) process [10, 13, 16]. This makes the integration of SIW and other planar circuitry on the board simple and cost-effective. Besides, it is claimed to perform better than microstrip structures at high frequencies and has the waveguide transmission performance [13]. Because of all of these properties and advantages, SIWs have been applied to several microwave components, including filters [17–18], directional couplers [19], oscillators [20], antennas [21] and circulators [22].

In the last years, many planar filter structures have been proposed in microstrip line and stripline form [23-24]. Such filters have advantages like low cost, small size, easy to integrate, but it has a low-quality factor (Q = 50-100). Although RW filters have many disadvantages, their quality factor is high (Q = 5000-10000). When the requirements such as integrability, low cost, small size, high power handling capability and low insertion loss are considered, SIW filters become a better alternative. SIW filters bridge the gap between microstrip line filters and RW filters by achieving a relatively high-quality factor (Q = 500-1000) [25].

Due to the properties and advantages of the SIW filters, this paper is contributed to design SIW BPFs that work at the X-band frequency range (8-12 GHz); these filters could be used in many applications including radar and satellite communications. The X-band has been chosen because it is used for a wide range of civil and military applications [26-27]. Moreover, it has extremely low rates of atmospheric attenuation in comparison to frequencies above 10 GHz, which makes this band suitable for the harshest weather conditions [28]. Although different types of SIW filters can be found in the literature [29-40], the design procedures are not given properly or are suited only for a specific filter order. This work discusses the design procedures of two different types of SIW BPFs in details; in particular the centered post and the iris types. Third and fifth-orders of both types have been simulated by taking into consideration two types of filter responses (Butterworth, Chebyshev). The design and simulation results of a third-order filter on different bandwidths are demonstrated, as well. All the simulations have been done using CST Microwave Studio. Post and iris third-order filters with Chebyshev response have been fabricated and scattering parameters of the prototypes are measured.

SIW FILTER DESIGN METHODOLOGY

In this part, the design steps of the centered post and iris SIW BPFs are discussed. In general, the design of the SIW itself starts from an equivalent RW. In this work, the equivalent RW is the WR-90 waveguide that works on the desired frequency band (X-band).

Fig. 1 shows the structure and dimensions of the SIW. In SIW design, we used copper and RT/Duroid 5870 dielectric material, which has a relative permittivity (ε_r = 2.33) and a loss tangent ($tan\ \delta$ = 0.0012 at 10 GHz). The procedure discussed in [10] is used to calculate the dimensions

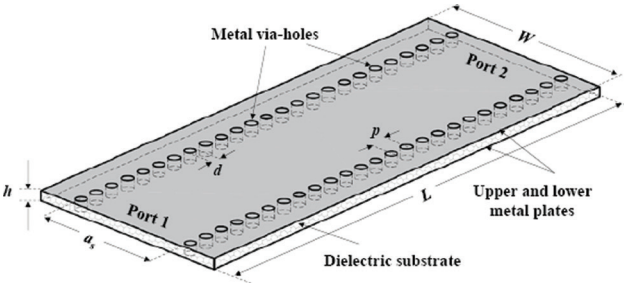

Figure 1. Structure and dimensions of the SIW.

of the corresponding SIW. To minimize the radiation loss of the SIW while designing it, the pitch length (p) and the via-hole diameter (d) should achieve the following conditions $d < \lambda_g/5$ and $p \leq 2d$, where λ_g is the guided wavelength [25, 32]. As a result, SIW dimensions are calculated as follows: L = 59.421 *mm*, W = 20 *mm*, a_s = 15.9028 *mm*, d = 1.3205 *mm*, p = 1.9807 *mm*. Note that the thickness of the substrate (h) is 1.57 *mm*.

Centered post SIW BPF design procedure

The design procedure of the centered post SIW filter shown in Fig. 2.a begins from the derivation of the equivalent RW filter. A post is a shunt inductance in the waveguide, which acts both as a cavity wall and as an impedance inverter coupling the adjacent cavities and it can be used to build RW BPFs [41]. Each post inside the RW has an equivalent circuit, as shown in Fig. 2.b [42].

It is known that the BPFs have a center frequency called (f_0) and the bandwidth (BW) of the filter is the difference between upper and lower cutoff frequencies ($BW = f_2 - f_1$). Eq. (1) describes the guide wavelength inside the RW in inches,

$$\lambda_g = \frac{1}{\sqrt{(0.08472 f)^2 - \left(\frac{1}{2a}\right)^2}} \tag{1}$$

where, a is the width of the RW and f is the frequency in GHz.

The guide wavelength at the center frequency (λ_{g_0}) is obtained by taking the arithmetic average of the guide wavelength at the lower frequency (λ_{g_1}) and upper frequency (λ_{g_2}). The equations for the frequency fractional bandwidth (w) and the guide wavelength fractional bandwidth (w_λ) are given in Eqs. (2) and (3), respectively.

$$w = \frac{f_2 - f_1}{f_0} \tag{2}$$

$$w_\lambda = \frac{\lambda_{g_1} - \lambda_{g_2}}{\lambda_{g_0}} = w\left(\frac{\lambda_{g_0}}{\lambda_0}\right)^2 \tag{3}$$

For the n^{th} order filter, we can calculate the element values of the filter (g_0, g_1,…, g_n, g_{n+1}) using the methods described in [42], or we can take it from the ready tables that are made for that. Note that, in our work, we are dealing with two responses of the filters, which are maximally flat (Butterworth) response and equal ripple (Chebyshev) response.

After determining the element values of the desired filter, we have to calculate the impedance inverter parameters ($K_{j,j+1}$) using Eqs. (4)-(6):

$$\frac{K_{01}}{Z_0} = \sqrt{\frac{\pi}{2}\frac{w_\lambda}{g_0 g_1 \omega_1'}} \tag{4}$$

$$\frac{K_{j,j+1}}{Z_0} = \frac{\pi w_\lambda}{2\omega_1'}\frac{1}{\sqrt{g_j g_{j+1}}}\bigg|_{j=1,2,\ldots\ldots,n-1} \tag{5}$$

$$\frac{K_{n,n+1}}{Z_0} = \sqrt{\frac{\pi}{2}\frac{w_\lambda}{g_n g_{n+1} \omega_1'}} \tag{6}$$

where, Z_0 is the guide impedance. The shunt reactance (X_b) can be obtained as follows:

$$\frac{X_{j,j+1}}{Z_0} = \frac{\frac{K_{j,j+1}}{Z_0}}{1 - \left(\frac{K_{j,j+1}}{Z_0}\right)^2} \tag{7}$$

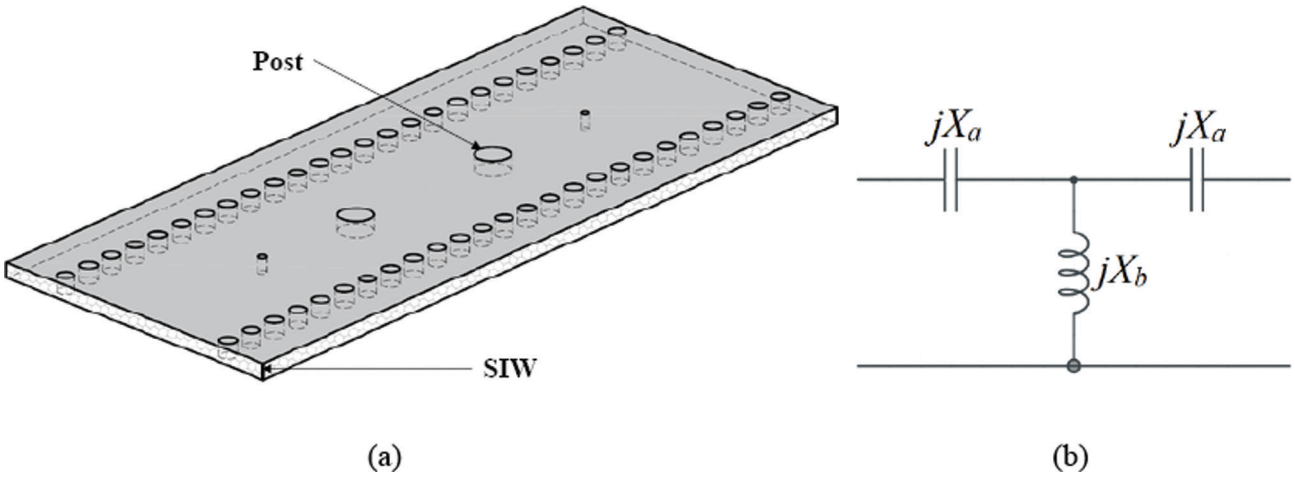

Figure 2. Centered post SIW filter (a) Its structure; (b) Equivalent circuit of a single post.

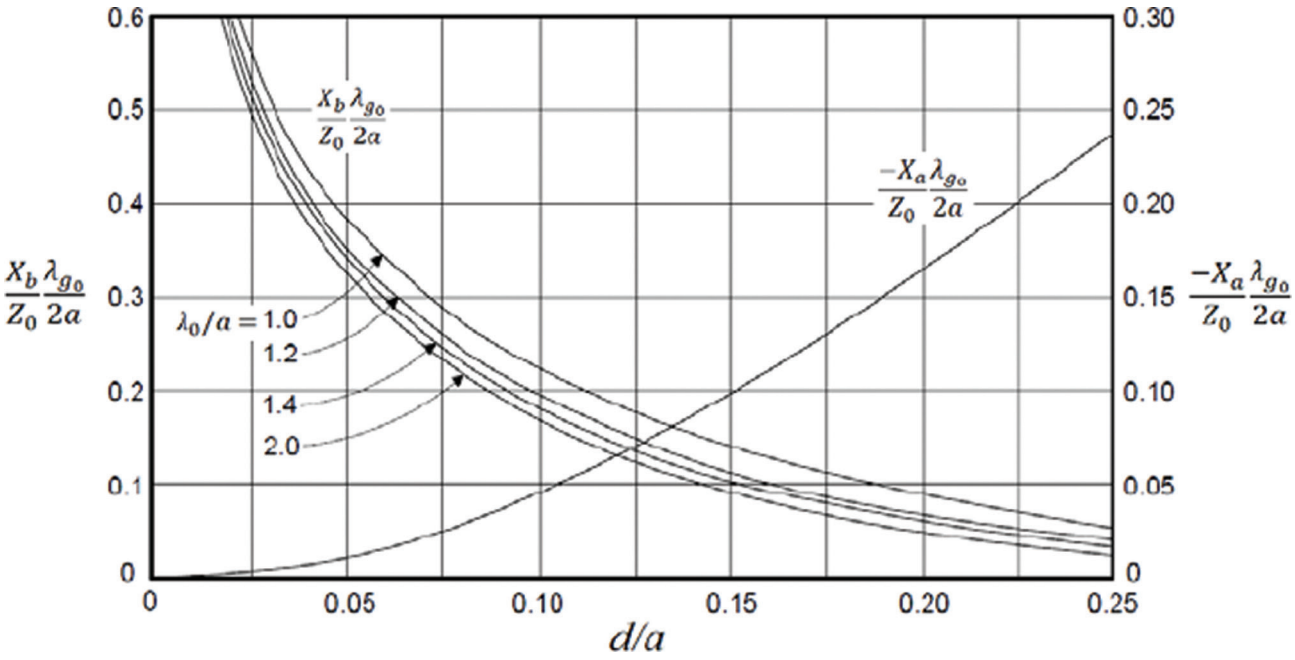

Figure 3. Circuit parameters of a centered inductive post in RW [42].

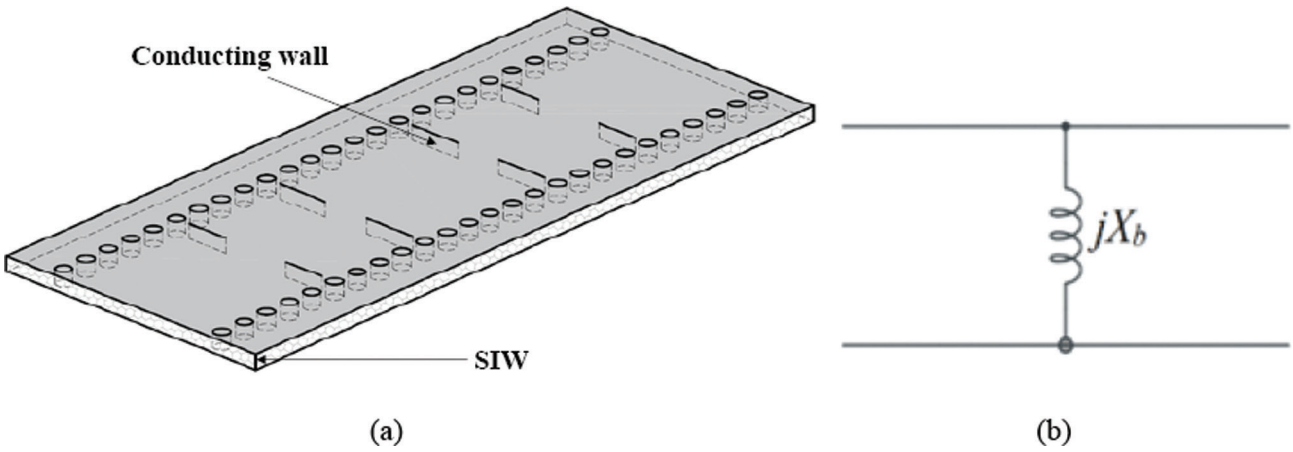

Figure 4. Iris SIW Filter (a) Filter structure with conducting walls; (b) Equivalent circuit of a single iris.

Circuit parameters of a centered inductive post in RW are exhibited in Fig. 3. λ_0/a value determines the approximate curve to be used. By using that curve and the $(X_b\lambda_{g_0})/(Z_0(2a))$ ratio, the diameter ($d_{j,j+1}$ where, j = 0,1,…,n) of each post is calculated. From the value of d/a and the inverse curve of $(-X_a\lambda_{g_0})/(Z_0(2a))$, X_a is calculated.

To calculate the distances between the centers of the posts (L_i) inside the filter, Eqs. (8)-(10) are used:

$$\theta_j = \pi + \frac{1}{2}\left[\phi_{j-1,j} + \phi_{j,j+1}\right] \tag{8}$$

$$\phi = -\tan^{-1}\left(\frac{2X_b}{Z_0} + \frac{X_a}{Z_0}\right) - \tan^{-1}\left(\frac{X_a}{Z_0}\right) \tag{9}$$

$$L_i = \frac{\lambda_{g_0}\theta_i}{2\pi} \tag{10}$$

Once post diameters and the distances between them are determined, centered post RW BPF can be converted to centered post SIW BPF by dividing all the dimensions by the square root of the relative permittivity of dielectric material used to design the SIW.

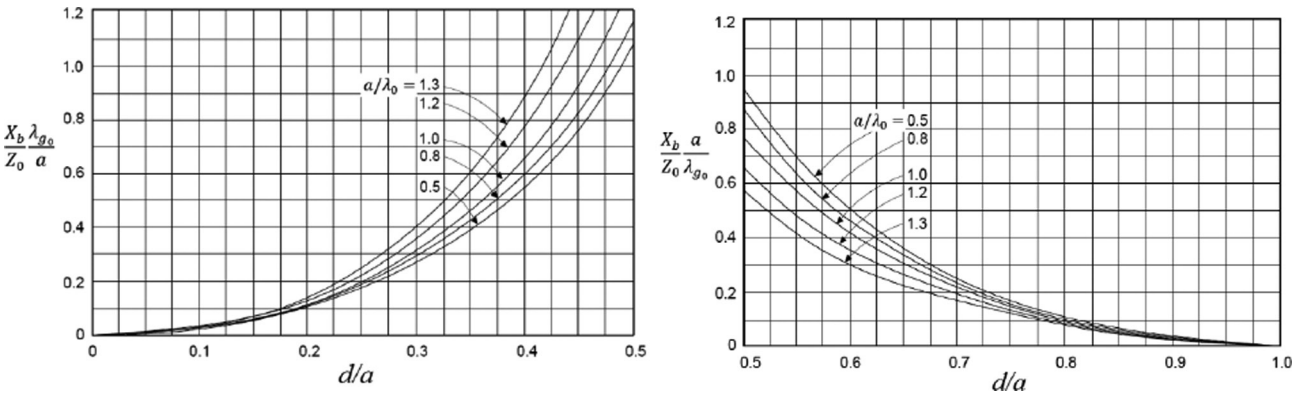

Figure 5. Shunt reactance of symmetrical inductive window in RW [42].

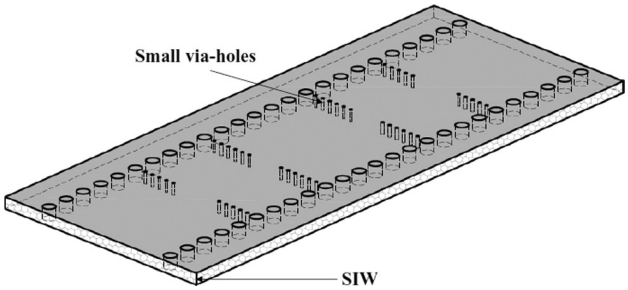

Figure 6. Iris SIW BPF structure using small via-holes.

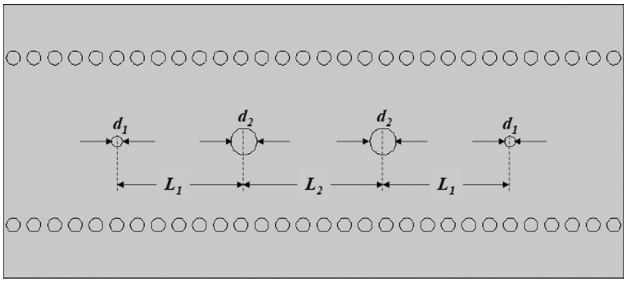

(a)

Figure 7.a Third order SIW Post filter dimensions.

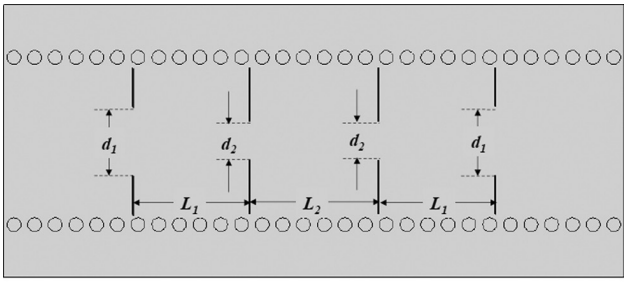

(b)

Figure 7.b Third order SIW Iris filter dimensions.

Iris SIW BPF design procedure

An iris is a conductive diaphragm placed transverse to a waveguide aperture that causes a discontinuity and generates shunt reactance and it can be used to build RW BPFs [41]. The design procedure of the iris SIW filter shown in Fig. 4.a begins from the derivation of the equivalent RW filter. The following procedure discusses the use of a thin iris, which has purely inductive characteristic, to build a BPF. Each thin iris inside the RW has an equivalent circuit, as shown in Fig. 4.b [42].

For purely lumped inductance iris having shunt reactance (X_b), the shunt reactance can be calculated using Eq. (7). Shunt reactance of symmetrical inductive window in RW are demonstrated in Fig. 5. a/λ_0 value determines the approximate curve to be used. By using that curve and the $(X_b\lambda_{g_0})/(Z_0(a))$ ratio or the $(X_b(a))/(Z_0\lambda_{g_0})$ ratio, the window width ($d_{j,j+1}$ where, $j = 0,1,\ldots,n$) of each iris is determined.

The distances between the irises (L_i) are calculated by using Eqs. (11) and (12):

$$\theta_j = \pi - \frac{1}{2}\left[\tan^{-1}\left(\frac{2X_{j-1,j}}{Z_0}\right) + \tan^{-1}\left(\frac{2X_{j,j+1}}{Z_0}\right)\right] \quad (11)$$

$$L_i = \frac{\lambda_{g_0}\theta_i}{2\pi} \quad (12)$$

When iris window width and distances between them are determined, iris RW BPF can be converted to iris SIW BPF by following the same procedure of post filter. Since the structure of SIW depends on using via-holes, copper walls in the iris SIW filter is rebuilt by the use of a line of small via-holes, as shown in Fig. 6. To keep the pure inductiveness of iris, the via-holes should have a small diameter of 0.2 *mm* with 0.6 *mm* separation between them.

SIW FILTERS ANALYSIS

In this section, the design and simulation results of both centered post and iris SIW BPFs are demonstrated.

Third-order and fifth-order filters with maximally flat and equal ripple responses are considered. Note that the simulated filters have a center frequency of 10 GHz and a bandwidth of 500 MHz. Moreover, the equal ripple response is assumed to be 0.1 dB ripple level. Fig. 7 shows the parameters of post and iris filters. Corresponding values for third and fifth-orders of the post and iris SIW BPFs dimensions are listed in Tables 1-2.

The simulation results of third-order filters are exhibited in Fig. 8. The maximally flat third-order centered post SIW filter achieves an insertion loss (IL) of 0.68 dB and a return loss (RL) of 45 dB at the center frequency. The IL and RL are equal to 6.15 dB and 2 dB at the upper frequency, respectively, whereas they are 3.5 dB and 5.16 dB at the lower frequency. For the maximally flat third-order iris SIW filter, it achieves IL and RL of 0.52 dB and 20 dB at the center frequency. The pit of the RL curve, which is at approximately 35 dB level, is shifted to 9.9 GHz for this case. The RL and IL are 5.4 dB and 2.8 dB at the upper frequency, respectively. They are 6.88 dB and 4.5 dB at the lower frequency. When RL and IL curves of post and iris filters are examined, wider bandwidth with lower insertion loss is observed for post filter. The equal ripple third-order centered post SIW filter achieves IL and RL of 0.78 dB and 23 dB at the center frequency. RL of the filter is below 17.5 dB at the upper half-band, whereas it is lower than 21.9 dB at the lower half-band. For the equal ripple third-order iris SIW filter, IL and RL are 0.89 dB and 21.23 dB at the center frequency, respectively. RL of the filter is below 24.5 dB at the upper half-band, whereas it is lower than 14.14 dB at the lower half-band. RL and IL curves of post and iris filters show that wider bandwidth with lower insertion loss is observed for post filter. Besides, lower insertion loss is observed at the lower and upper frequencies of the band with equal ripple response.

The transmission characteristics (insertion loss and return loss) of the demonstrated SIW filters are almost identical to the equivalent RW filters' characteristics as well. The numerical simulation results for third-order SIW filters are given in Table 3 clearly.

The equal ripple fifth-order centered post SIW filter achieves IL and RL of 0.2 dB and 32 dB at the center frequency, respectively. It achieves RL better than 17.44 dB

Table 1. Third-order post and iris SIW BPFs dimensions

Centered post SIW filter dimensions (mm)				
	d_1	d_2	L_1	L_2
Maximally flat response	0.6839	2.6092	11.8278	13.4635
Equal ripple response	0.7056	2.2498	11.5898	12.9377
Iris SIW filter dimensions (mm)				
	d_1	d_2	L_1	L_2
Maximally flat response	6.5529	3.6342	11.1705	12.2438
Equal ripple response	6.5046	4.0802	11.0723	12.0042

Table 2. Equal ripple fifth-order SIW BPFs dimensions

Centered post SIW filter dimensions (mm)					
d_1	d_2	d_3	L_1	L_2	L_3
0.7821	2.4461	2.8122	11.8161	13.4868	13.7464
Iris SIW filter dimensions (mm)					
d_1	d_2	d_3	L_1	L_2	L_3
6.3682	3.8539	3.4179	11.2304	12.2704	12.3769

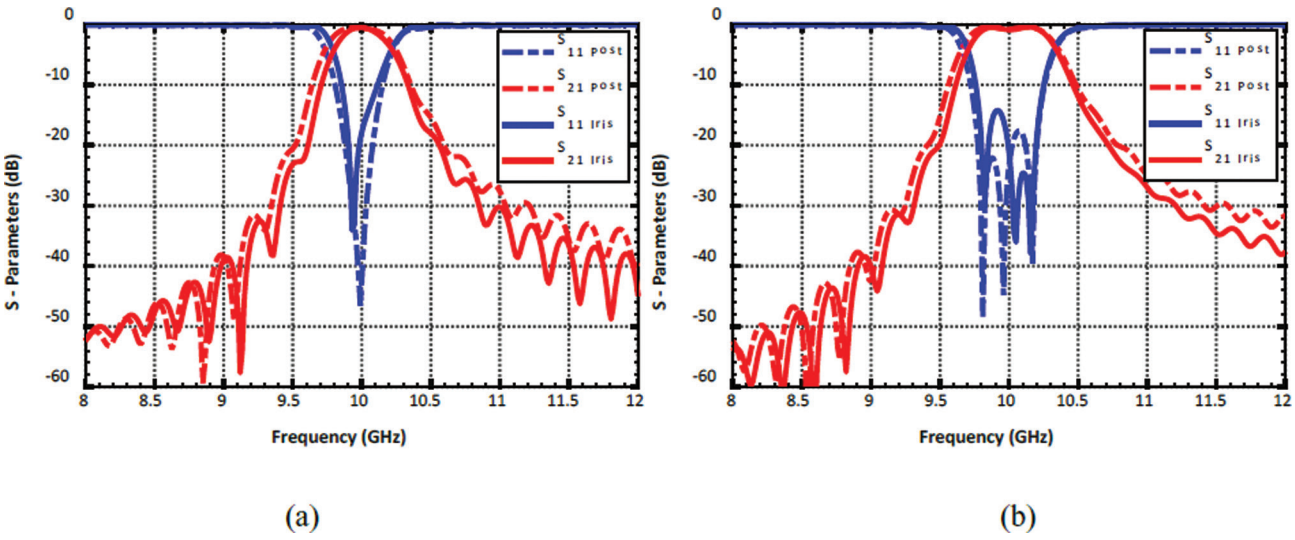

Figure 8. Scattering parameters of the 3rd order centered post and iris SIW BPFs (a) Maximally flat response; (b) Equal ripple response.

Table 3. Numerical simulation results for (a) 3rd order post SIW filters; (b) 3rd order iris SIW filters

(a)

Frequency response	**Maximally flat**			**Equal ripple**		
Frequency	Lower cutoff frequency	Center frequency	Upper cutoff frequency	Lower cutoff frequency	Center frequency	Upper cutoff frequency
Insertion loss (dB)	3.5	0.68	6.15	1.23	0.78	1.33
Return loss (dB)	5.16	45	2	14	23	10.7

(b)

Frequency response	**Maximally flat**			**Equal ripple**		
Frequency	Lower cutoff frequency	Center frequency	Upper cutoff frequency	Lower cutoff frequency	Center frequency	Upper cutoff frequency
Insertion loss (dB)	6.88	0.52	5.4	2.33	0.89	1.43
Return loss (dB)	4.5	20	2.8	8.79	21.23	10.11

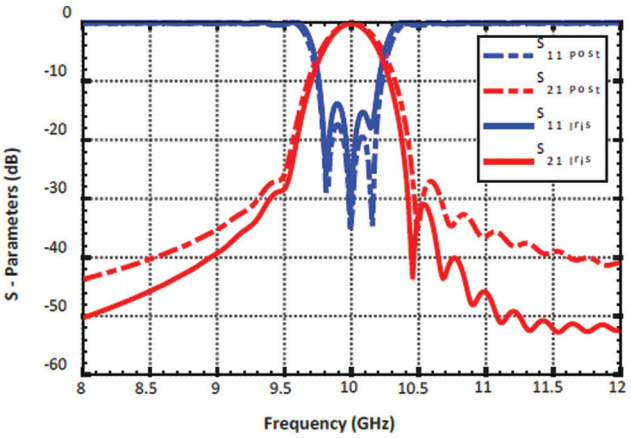

Figure 9. Scattering parameters of the 5th order centered post and iris SIW BPFs with equal ripple response.

in the whole band. For the equal ripple fifth-order iris SIW filter, IL and RL are observed as 0.21 dB and 28 dB at the center frequency. It achieves a RL better than 14 dB in the whole band. IL at band extremes is lower for post filter. Although the IL of the 5th order filter is higher at the upper and lower frequencies of the band compared to 3rd order filter, steep-skirt selectivity of the 5th order filter is easily observed. The numerical simulation results for equal ripple fifth-order SIW filters are given in Table 4 clearly.

Finally, simulation results of the third-order iris SIW BPFs with 0.1 dB equal ripple response, designed by applying the above mentioned procedure, are shown in Fig. 10 for different bandwidths. The figure clearly shows that the increase in the bandwidth results in higher insertion loss at the stop-bands of the filter. To demonstrate the usefulness of small via-holes instead of copper walls, third-order iris SIW filter with equal ripple response is designed with both structures and simulation results are exhibited in Fig. 11. Filter with via-holes achieves IL and RL of 0.81 dB and 30 dB at the center frequency, respectively. Although insertion losses of the two filters are very close to each other at the pass-band of the filter, its level is lower at the stop-bands of the filter with via-holes. Thus, using small via-holes instead of copper walls does not affect the general performance and characteristics of the filter considerably.

Table 5 includes a comparison of iris and post filters with other filters in the literature. In general, the simulation results of the proposed filters achieve an insertion loss and a return loss better than the filters found in [31-32, 43-45]. Furthermore, two types of frequency responses (Butterworth, Chebyshev) are included and we have proposed filters with fifth-order which is not included in the literature.

EXPERIMENTAL VERIFICATION

This section shows and discusses the measured results of two fabricated SIW filters. One of them has been fabricated using post type, and the other using the iris type. The fabricated filters are third-order filters with 0.1 dB equal ripple response whose dimensions are given in Table 1. Prototypes are fabricated by chemical etching technique with via-hole coating. Rogers RT/Duroid 5870 (ε_r = 2.33) substrate with 1.57 *mm* dielectric thickness and 35 μm copper thickness is used. Tapered microstrip line is used for the transition between 50 Ω SMA (sub-miniature assembly) connector and SIW filter. The size of the filters is 96.4 *mm* × 20 *mm* (*lenght* × *width*). Fabricated prototypes are given in Fig. 12. The top and bottom sides of post filter is shown at the upper side, whereas iris filter is given below. Both filters have the advantages of small size, low cost, integrability,

Table 4. Numerical simulation results for 5th order SIW equal ripple filters

Filter type	Post			Iris		
Frequency	Lower cutoff frequency	Center frequency	Upper cutoff frequency	Lower cutoff frequency	Center frequency	Upper cutoff frequency
Insertion loss (dB)	5.75	0.2	5.55	6.95	0.21	7.67
Return loss (dB)	10.5	32	7.14	8.92	28	4.8

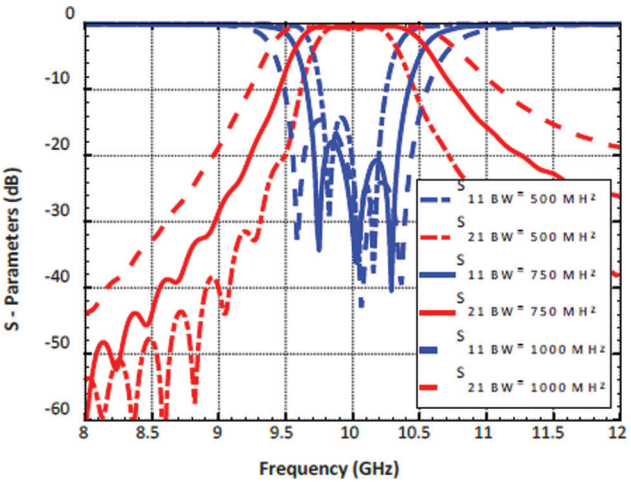

Figure 10. Scattering parameters of the 3rd order iris SIW BPF with different bandwidths.

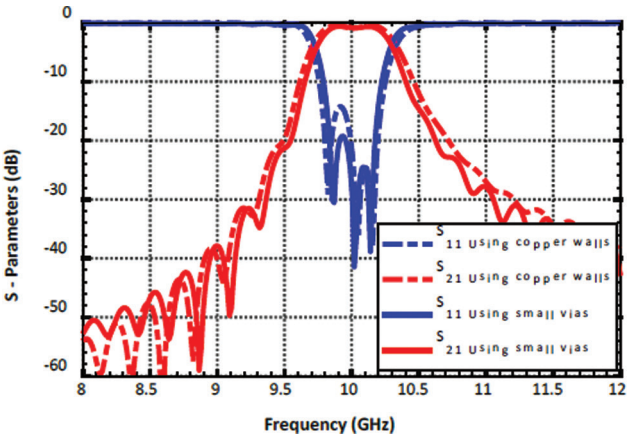

Figure 11. Comparison of scattering parameters for the iris SIW BPF with copper walls and conductor via-holes.

Table 5. Comparison of iris and post filters with other filters in literature

	Reference [31]	Reference [32]	Reference [43]	Reference [44]	Reference [45]	Proposed iris filter	Proposed post filter
Structure	Iris using via-holes	Offset post	SIFW	SIW cavity	SICC/SIEC	Iris	Centered post
Center frequency	12 GHz	28 GHz	10 GHz	10 GHz	10 GHz	10 GHz	10 GHz
Bandwidth	360 MHz	1 GHz	150 MHz	300 MHz	350 MHz	500 MHz	500 MHz
Amplitude response	Chebyshev	Chebyshev	Chebyshev	Elliptic	Elliptic	Butterworth, Chebyshev	Butterworth, Chebyshev
Physical size	29.68 mm × 6.22 mm	Not available	Not available	Not available	Not available	96.4 mm × 20 mm	96.4 mm × 20 mm
Dielectric substrate	Rogers RT/ Duroid 6010LM	Rogers RT/ Duroid 5880	Not available	Rogers RT/ Duroid 5880	Rogers RT/ Duroid 5880	Rogers RT/ Duroid 5870	Rogers RT/ Duroid 5870
Order of the filter	3rd	3rd	3rd	3rd	2nd	3rd, 5th	3rd, 5th
Insertion loss at the center frequency	2.03 dB	1 dB	2.7 dB	3.13 dB	1.65 dB	0.89 dB*	0.78 dB*
Return loss at the center frequency	30 dB	17 dB	20 dB	13.5 dB	19.5 dB	21.23 dB*	23 dB*

*The results belong to 3rd order Chebyshev filters.

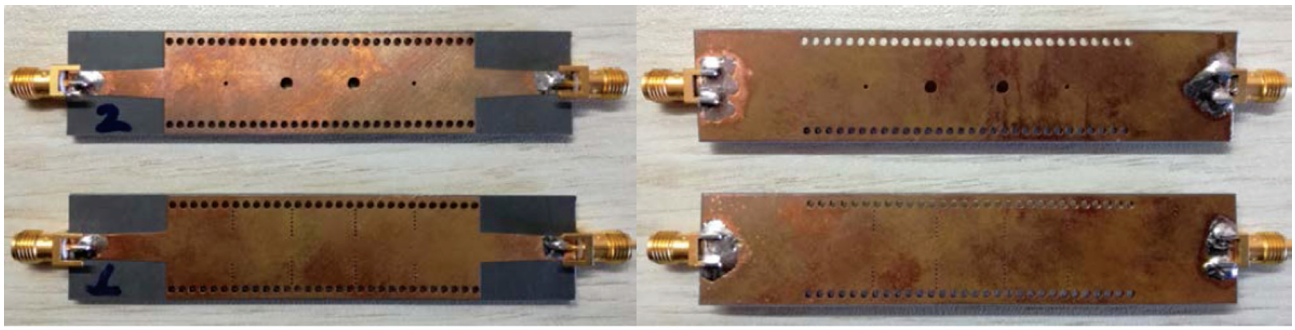

(a) (b)

Figure 12. Fabricated prototypes (a) Top view; (b) Bottom view.

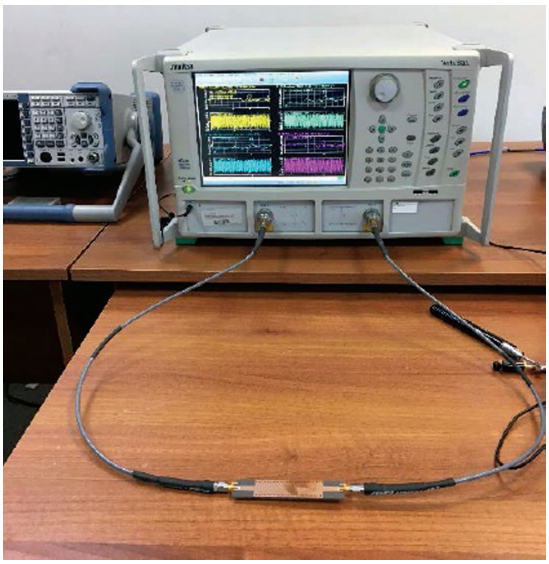

Figure 13. Measurement setup.

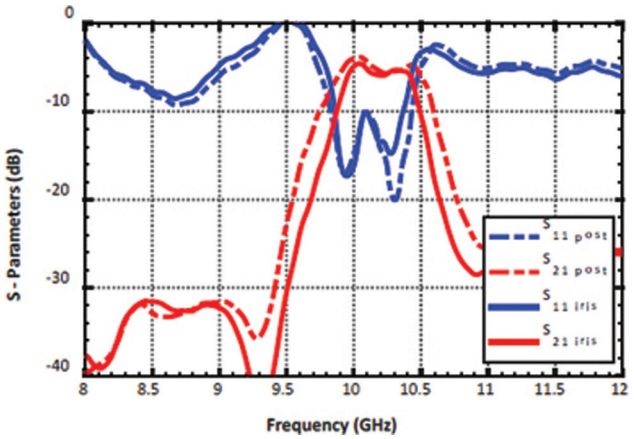

Figure 14. Measured scattering parameters of the 3rd order centered post and iris SIW BPFs with equal ripple response.

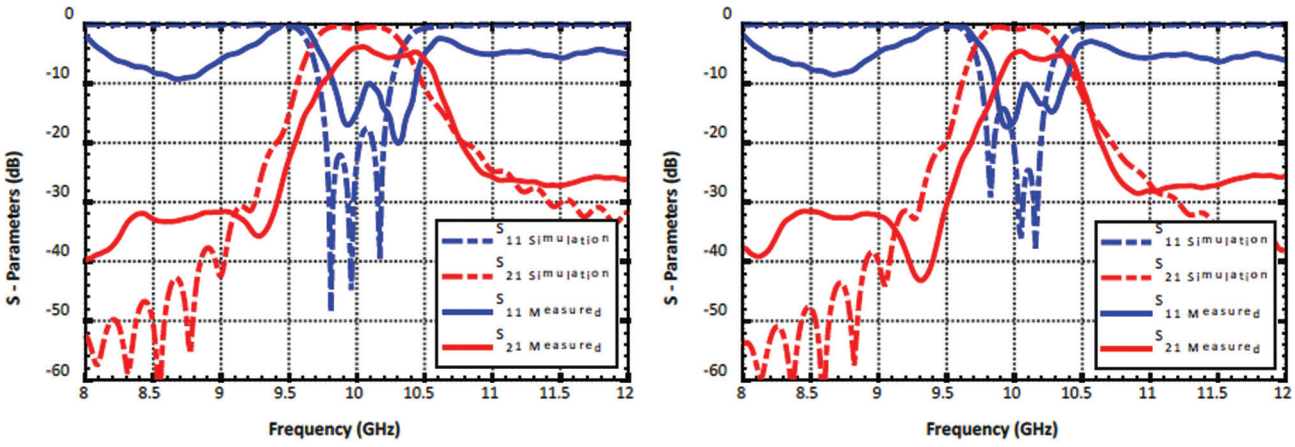

(a) (b)

Figure 15. Measured and simulated results of the 3rd order SIW BPFs with equal ripple response (a) Post type; (b) Iris type.

high performance but the manufacturing of the iris filter is more difficult compared to the post filter.

Anritsu network analyzer is used to measure the characteristics of the filters. The measurement setup is demonstrated in Fig. 13. Reflection and transmission behavior of the filters are observed by S_{11} and S_{21}. Measured scattering parameters of fabricated filters are given in Fig. 14. Measured insertion loss is around 4 dB levels at the pass-band of the filter. This high loss which was not observed at the simulations is attributed to cable and connector losses at the measurement setup. The fabrication tolerances for the via-holes have an impact on this loss level, as well. RL and IL curves of post and iris filters show that wider bandwidth with lower insertion loss is observed for post filter. Besides, lower insertion loss is observed at the lower and upper frequencies of the band with equal ripple response. This conclusion was observed in the simulations, as well.

Finally, the comparison of measured and simulated results for both fabricated SIW filters is demonstrated in Fig. 15. The discrepancy between the real performance and the simulation results lies in the difference between the real object and its assumed model. The behavior of the filter is ideal within the defined bounding box, whereas the measurements are conducted at a laboratory where external disturbances exist. Besides, cable and connector losses are included at the measurement setup. The fabrication tolerances of the SIW filter have an impact on this loss level, as well. Although this loss level is critical in real-life applications, the measurement results still able us to make a comparison between the general characteristics of post and iris filters.

CONCLUSIONS

In this paper, the design procedure for the widely used post and iris RW filters in SIW form is given. The methodology is applied to post and iris SIW filters with different orders, responses and bandwidths. By following the procedure, very similar reflection and transmission characteristics to that of post and iris RW filters are obtained with SIW filters. The designs are simulated by means of a full-wave simulator. Both types of SIW filters work on 10 GHz center frequency and 500 MHz bandwidth. Moreover, in simulations of third-order Chebyshev filters, the iris SIW filter achieves lower than 0.89 dB insertion loss and better than 21.23 dB return loss in the pass-band. Whereas the post SIW filter achieves lower than 0.78 dB insertion loss and better than 23 dB return loss in the pass-band. The characteristics of the post and iris SIW filters are compared by both simulation and measurement results. The filters exhibit low insertion loss and high reflection loss at the stop-band of the filter. With their low cost, small size, ease of manufacturing, high performance and integrability with other components, both of the demonstrated X-band SIW filters are very versatile and well suited for a variety of market applications, including radars and satellite communications. Especially the post filters because they have an easy fabrication process comparing to the fabrication of iris filters. This work can be extended by adjusting the size of the posts tunable, which enables the user to change the center frequency and the bandwidth slightly, or the shape of the filter response.

AUTHORSHIP CONTRIBUTIONS

Authors equally contributed to this work.

DATA AVAILABILITY STATEMENT

The authors confirm that the data that supports the findings of this study are available within the article. Raw data that support the finding of this study are available from the corresponding author, upon reasonable request.

CONFLICT OF INTEREST

The author declared no potential conflicts of interest with respect to the research, authorship, and/or publication of this article.

ETHICS

There are no ethical issues with the publication of this manuscript.

REFERENCES

[1] Pozar DM. Microwave Engineering. 4th ed. Hoboken, NJ, USA: John Wiley & Sons, 2011: 95–450.

[2] Cameron RJ, Kudsia CM, Mansour RR. Microwave filters for communication systems: Fundamentals, design, and applications. 2nd ed. Hoboken, NJ, USA: John Wiley & Sons, 2018:1–74. [CrossRef]

[3] Herter Jr, CA. The electromagnetic spectrum: A critical natural resource. Nat Res J 1985;25:651–663.

[4] Teberio F, Percaz JM, Arregui I, Martin-Iglesias P, Lopetegi T, Laso MA, et al. Rectangular waveguide filters with meandered topology. IEEE Trans Microw Theory Tech 2018;66:3632–3643. [CrossRef]

[5] Oncu E, Dudak C, Akan V, Topalli K. A compact filter using substrate integrated waveguide technology, 6th International Conference on Recent Advances in Space Technologies, Istanbul, Turkey, 2013:527–530. [CrossRef]

[6] Bastioli S, Marcaccioli L, Sorrentino R. Compact dual-mode rectangular waveguide filters using square ridge resonators. Int J Microw Wirel Technol 2009;1:241. [CrossRef]

[7] Rhbanou A, Bri S. Design of substrate integrated

waveguide pass filter at 33-75 GHz band. Int J Eng Technol 2014;6:2815–2825.

[8] Deslandes D, Wu K. Integrated microstrip and rectangular waveguide in planar form. IEEE Microw Wirel Compon Lett 2001;11:68–70. [CrossRef]

[9] Rayas-Sanchez JE, Gutierrez-Ayala V. A general EM-based design procedure for single-layer substrate integrated waveguide interconnects with microstrip transitions. IEEE MTT-S International Microwave Symposium, Atlanta, GA, USA, 2008:983–986. [CrossRef]

[10] Rabah MA, Abri M, Tao J, Vuong TH. Substrate integrated waveguide design using the two dimentionnal finite element method. Prog Electromagn Res M 2014;35:21–30. [CrossRef]

[11] Bozzi M, Perregrini L, Wu K. Modeling of conductor, dielectric, and radiation losses in substrate integrated waveguide by the boundary integral-resonant mode expansion method. IEEE Trans Microw Theory Tech 2008;56:3153–3161. [CrossRef]

[12] Bozzi M, Perregrini L, Wu K. Modeling of losses in substrate integrated waveguide by boundary integral-resonant mode expansion method, IEEE MTT-S International Microwave Symposium, Atlanta, GA, USA, 2008:515–518. [CrossRef]

[13] Bozzi M, Georgiadis A, Wu K. Review of substrate-integrated waveguide circuits and antennas. IET Microw Antennas Propag 2011;5:909–920. [CrossRef]

[14] Deslandes D, Wu K. Accurate modeling, wave mechanisms, and design considerations of a substrate integrated waveguide. IEEE Trans Microw Theory Tech 2006;54:2516–2526. [CrossRef]

[15] Tan Q, Guo Y, Zhang L, Lu F, Dong H, Xiong J. Substrate integrated waveguide (SIW)-based wireless temperature sensor for harsh environments. Sensors J 2018;18:1406. [CrossRef]

[16] Xu F, Wu K. Guided-wave and leakage characteristics of substrate integrated waveguide. IEEE Trans Microw Theory Tech 2005;53:66-73. [CrossRef]

[17] Chen X, Hong W, Cui T, Chen J, Wu K. Substrate integrated waveguide (SIW) linear phase filter. IEEE Microw Wirel Compon Lett 2005:15:787–789. [CrossRef]

[18] Chen XP, Wu K, Li ZL. Dual-band and triple-band substrate integrated waveguide filters with Chebyshev and quasi-elliptic responses. IEEE Trans Microw Theory Tech 200;55:2569–2578. [CrossRef]

[19] Hao ZC, Hong W, Chen JX, Zhou HX, Wu K. Single-layer substrate integrated waveguide directional couplers. IET Microw Antennas Propag 2006;153:426–431. [CrossRef]

[20] Cassivi Y, Wu K. Low cost microwave oscillator using substrate integrated waveguide cavity. IEEE Microw Wirel Compon Lett 2003;13:48–50. [CrossRef]

[21] Henry M, Free CE, Izqueirdo BS, Batchelor J, Young P. Millimeter wave substrate integrated waveguide antennas: Design and fabrication analysis. IEEE Trans Adv Packag 2009;32:93–100. [CrossRef]

[22] D'Orazio W, Wu K. Substrate-integrated-waveguide circulators suitable for millimeter-wave integration. IEEE Trans Microw Theory Tech 2006;54:3675–3680. [CrossRef]

[23] Hsu CL, Hsu FC, Kuo JK. Microstrip bandpass filters for ultra-wideband (UWB) wireless communications, IEEE MTT-S International Microwave Symposium, Long Beach, CA, USA, 2005:4.

[24] Mobbs CI, Rhodes JD. A generalized Chebyshev suspended substrate stripline bandpass filter. IEEE Trans Microw Theory Tech 1983;31:397–402. [CrossRef]

[25] Deslandes D. Design equations for tapered microstrip-to-substrate integrated waveguide transitions. IEEE MTT-S International Microwave Symposium, Anaheim, California, USA, 2010:704–707. [CrossRef]

[26] Nwosu RI. A comparative study of LiFi and other data transfer mediums. Curr J Appl Sci Technol 2019;38:1–7. [CrossRef]

[27] Tripathi AK, Singh BK. A CPW fed x-band antenna for satellite & radar applications, international conference on microwave and photonics (ICMAP), India, 2013:1–3.

[28] Rodriquez S, Heymsfield G, Li L, Bradley D. X-Band Radar for Studies of Tropical Storms from High Altitude UAV Platform, Geoscience and Remote Sensing Symposium, Barcelona, 2007.

[29] Zhao C, Fumeaux C, Kaufmann T, Zhu Y, Horestani AK, Lim CC. A general design method for band-pass post filters in rectangular waveguide and substrate integrated waveguide, International Symposium on Antennas and Propagation (ISAP), Hobart, Tasmania, Australia, 2015:1–4.

[30] Sangam RS, Kshetrimayum RS. Approximate design equation for Iris width calculation of Iris Substrate Integrated Waveguide (SIW) bandpass filters, Twenty-third National Conference on Communications (NCC), Chennai, India, 2017:1–3. [CrossRef]

[31] Yun TS, Nam H, Kim KB, Lee JC. Iris waveguide bandpass filter using substrate integrated waveguide (SIW) for satellite communication, Asia-pacific microwave conference, Suzhou International Conference Center, Suzhou, China, 2005:4.

[32] Deslandes D, Wu K. Single-substrate integration technique of planar circuits and waveguide filters, IEEE transactions on microwave theory and techniques 2003;51:593–596. [CrossRef]

[33] Nguyen NH, Parment F, Ghiotto A, Wu K, Vuong TP. A fifth-order air-filled SIW filter for future 5G applications. 2017 IEEE MTT-S International

Microwave Workshop Series on Advanced Materials and Processes for RF and THz Applications (IMWS-AMP), Pavia, Italy, 2017:1–3. [CrossRef]

[34] Celis S, Farhat M, Almansouri AS, Bagci H, Salama KN. Simplified modal-cancellation approach for substrate-integrated-waveguide narrow-band filter design. Electronics 2020;9:962. [CrossRef]

[35] Parment F, Ghiotto A, Vuong TP, Duchamp JM, Wu K. Low-loss air-filled substrate integrated waveguide (SIW) band-pass filter with inductive posts, 2015 European Microwave Conference (EuMC), Paris, France, 2015, 761–764. [CrossRef]

[36] Nwajana AO, Dainkeh A, Yeo KS. Substrate integrated waveguide (SIW) bandpass filter with novel microstrip-CPW-SIW input coupling. Journal of Microwaves, Optoelectronics and Electromagnetic Applications 2017;16:393–402. [CrossRef]

[37] Chen XP, Wu K. Substrate integrated waveguide filters: Design techniques and structure innovations. IEEE Microw Mag 15(6), 121–133, 2014. [CrossRef]

[38] Tomassoni C, Silvestri L, Ghiotto A, Bozzi M, Perregrini L. Substrate-integrated waveguide filters based on dual-mode air-filled resonant cavities. IEEE Trans Microw Theory Tech 2018;66:726–736. [CrossRef]

[39] Huang Y, Shao Z, Liu L. A substrate integrated waveguide bandpass filter using novel defected ground structure shape. Prog Electromagn Res 2013;135:201–213. [CrossRef]

[40] Rhbanou A, Bri S, Sabbane M. Design of X-band substrate integrated waveguide bandpass filter with dual high rejection. Microw Opt Technol Lett 2015;57:1744–1752. [CrossRef]

[41] Bianchi G, Sorrentino R. Electronic filter simulation & design. 1st ed. New York, USA: McGraw Hill Professional, 2007:527–592.

[42] Matthaei GL, Young L, Jones EMT. Microwave filters, impedance-matching networks, and coupling structures. 2nd ed. Dedham, USA: Artech House, 1980:83–519.

[43] Wang Z, Shen D, Xu R, Yan B, Lin W. A partial H-plane substrate integrated folded waveguide (SIFW) bandpass filter based on H-plane slot. J Electromagn Waves Appl 2010;24:113–121. [CrossRef]

[44] Ismail A, Razalli MS, Mahdi MA, Raja Abdullah RSA, Noordin NK, Rasid MFA. X-band trisection substrate-integrated waveguide quasi-elliptic filter. Prog Electromagn Res 2008;85:133–145. [CrossRef]

[45] Zhang ZG, Fan Y, Cheng YJ, Zhang YH. A novel multilayer dual-mode substrate integrated waveguide complementary filter with circular and elliptic cavities (SICC and SIEC). Prog Electromagn Res 2012;127:173–188. [CrossRef]